ARTICLE

Unusual Electric and Optical Tuning of KTaO₃-Based Two-Dimensional Electron Gases with 5d Orbitals

Hui Zhang,[†,‡] Xi Yan,[†,‡] Xuejing Zhang,[†,‡] Shuai Wang,[§] Changmin Xiong,[§] Hongrui Zhang,[†,‡] Shaojin Qi,[†,‡] Jine Zhang,[†,‡] Furong Han,[†,‡] Ning Wu,[†,‡] Banggui Liu,[†,‡] Yuansha Chen,[†,‡] Baogen Shen,[†,‡] and Jirong Sun*,[†,‡]

[†]Beijing National Laboratory for Condensed Matter Physics, Institute of Physics, Chinese Academy of Sciences, Beijing 100190, Peoples' Republic of China

[‡]School of Physical Sciences, University of Chinese Academy of Sciences, Beijing 100049, Peoples' Republic of China

[§]Department of Physics, Beijing Normal University, Beijing 100875, Peoples' Republic of China

S Supporting Information

ABSTRACT: Controlling electronic processes in low-dimension electron systems is centrally important for both fundamental and applied researches. While most of the previous works focused on SrTiO₃-based two-dimensional electron gases (2DEGs), here we report on a comprehensive investigation in this regard for amorphous-LaAlO₃/ KTaO₃ 2DEGs with the Fermi energy ranging from ∼13 meV to ∼488 meV. The most important observation is the dramatic variation of the Rashba spin−orbit coupling (SOC) as Fermi energy sweeps through 313 meV: The SOC effective field first jumps and then drops, leading to a cusp of ∼2.6 T. Above 313 meV, an additional species of mobile electrons emerges, with a 50-fold enhanced Hall mobility. A relationship between spin relaxation distance and the degree of band filling has been established in a wide range. It indicates that the maximal spin precession length is ∼70.1 nm and the maximal Rashba spin splitting energy is ∼30 meV. Both values are much larger than the previously reported ones. As evidenced by density functional theory calculation, these unusual phenomena are closely related to the distinct band structure of the 2DEGs composed of 5d electrons. The present work further deepens our understanding of perovskite conducting interfaces, particularly those composed of 5d transition-metal oxides.

KEYWORDS: *two-dimensional electron gas, oxide interfaces, gating effect, optical gating, spin−orbital coupling*
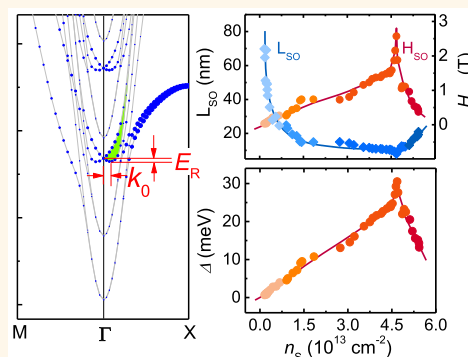
S ince its first discovery in 2004,[1] two-dimensional electron gases (2DEGs) at the LaAlO₃/SrTiO₃ (LAO/ STO) interfaces have attracted increasing attention, and exotic phenomena are observed,[1−13] including two-dimensional superconductivity at low temperatures,[5] interfacial magnetism persisting to room temperature,[11] and efficient spin-to-charge conversion.[12,13] After intensive investigations, it becomes more and more clear that approaches toward an effective tuning to the 2DEGs are the key to uncover the emergent phenomena at conducting oxide interfaces. Effects of field gating[7−9] and photo exciting[14−17] are proven effective to control the physical process in 2DEGs. As already demonstrated, gate field can trigger a switch of the 2DEG between a metallic and an insulating state.[7] Electric or optical tuning to the Rashba spin−orbit coupling (SOC), particularly gate-bias-caused variation in interfacial magnetism, was also reported for 2DEGs.[10,17−20]

We noticed that most of the previous investigations focused on 3d electron gases, that is, the 2DEGs residing in STO. In fact, there is an important species of electron gases, that is, the 2DEGs formed by 5d electrons at the ABO₃/KTaO₃ (KTO) interfaces. Although KTO is similar to STO with high permittivity and quantum paraelectricity, it is distinct for its strong atomic spin−orbit interaction that is nearly 20-fold as large as that of STO.[21,22] This will certainly affect the hierarchic band structure of the corresponding 2DEGs. Also, the electronic correlation should be different for KTO and STO due to the different characters of the 5d and 3d electrons. Therefore, distinct properties are expected for KTO-based 2DEGs.

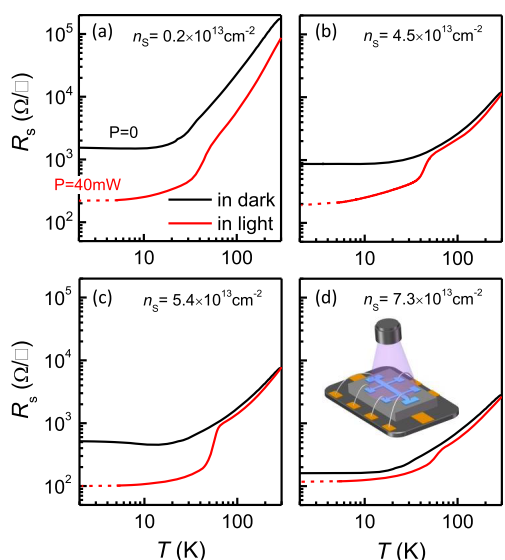Unfortunately, works on this kind of 2DEGs are scarce because of the difficulties to generate 2DEGs by interface engineering. In addition to a few examples of 2DEGs created by electric gating, ionic, or UV light irradiation,[23−26] the only reported 2DEGs at bilayer interfaces are LaTiO$_3$/KTO[27] and amorphous-LAO/KTO.[28] Effects associated with the distinct characters of KTO are far from being fully explored. Here we report on an unusual tuning effect of electric gating and photo exciting on KTO-based 2DEGs with totally different carrier density, thus Fermi energy. The effective fields related to spin−orbit scattering and inelastic scattering are determined as the Fermi energy of the 2DEGs sweeps from ∼11 meV to ∼362 meV, driven by successive electric and optical tuning. The most interesting observation is the presence of a critical level for band filling where Rashba spin−orbit coupling exhibits a cusp and a second species of charge carriers with a 50-fold enhanced Hall mobility emerges. As evidenced by density functional theory calculation, these unusual observations stem from the distinct hierarchic band structure of KTO-based 2DEGs.

RESULTS AND DISCUSSION

A series of 5d 2DEGs with the carrier densities (n_S) ranging from ∼0.2 × 10^{13} cm^{-2} to ∼7.3 × 10^{13} cm^{-2}, or the Fermi energy ($E_F = n_S h^2/4\pi m_e$ with h being Planck's constant and m_e = 0.36m_0 with m_0 being electron mass) from ∼13 meV to ∼488 meV were fabricated at the a-LAO/KTO interface following the procedures described in the Experimental Section (also see Supporting Information Figure S1 and Table S1). The widely spread Fermi energy allows a full exploration for the response of the 2DEGs in different states to electrostatic or optical gating. Figure 1 presents the temperature dependence of the sheet resistance (R_S) of different a-LAO/KTO interfaces, arranged in the order of carrier density. The oxide interfaces are well metallic over the whole
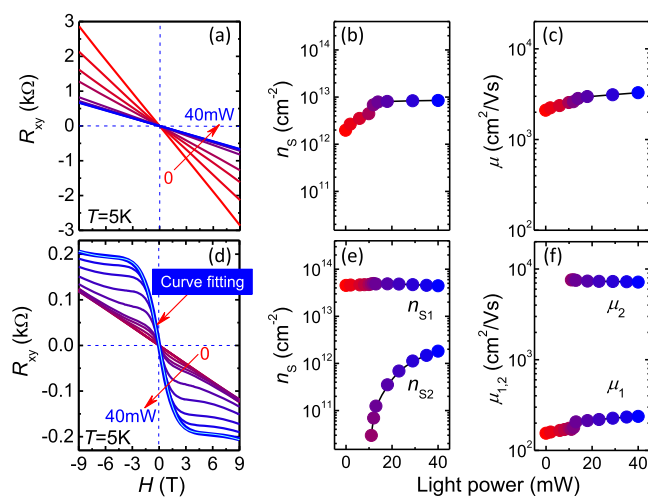
temperature range from 2 to 300 K, with an expected increase in overall resistance with the decrease of carrier density. These results together with the rectify-shaped anisotropic magneto-resistance (Supporting Information Figure S2) confirm the formation of 2DEGs at the a-LAO/KTO interfaces.

To get a general idea on the effect of photo excitation, in Figure 1 we also show the R_S-T curves obtained after light illumination (light power P = 40 mW and wavelength λ = 405 nm). As expected, the sheet resistance displays a sizable decrease when exposed to light. This effect is particularly strong for the samples with low carrier densities. For the 2DEG with a n_S of 0.2 × 10^{13} cm^{-2}, for example, the sheet resistance at 2 K decreases from ∼1540 Ω/□ to ∼221 Ω/□. In contrast when n_S is ∼7.3 × 10^{13} cm^{-2}, photo excitation only causes a R_S change from ∼161 Ω/□ to ∼118 Ω/□. These results are understandable: The excited electron density could be comparable to the equilibrium one when n_S is low. Thus, the illumination effect is much stronger. An unexpected observation is the illumination-induced sudden drop in R_S below 50 K. We found that the resistance of the bare KTO substrate also displays a considerable decrease at the same temperature when illuminated (Supporting Information Figure S3). This indicates that considerable photocarriers can be produced only below 50 K. However, the resistance of the KTO substrate is much greater than that of the a-LAO/KTO interface (∼270,000 Ω/□ versus ∼200 Ω/□ at 5 K). It means that the photocarriers dispersed in bulk KTO have negligible contributions to electronic transport due to their short lifetime. Only those photocarriers that are in or close to the interfacial region of the 2DEGs contribute to sheet conductance, that is, the electron gas remains 2D under light illumination.

To see what has happened to the 2DEG in light, the Hall effect of the 2DEGs is further investigated. Figure 2a,d show the Hall resistance (R_{XY}) for two typical 2DEGs, one with the lowest carrier density (0.2 × 10^{13} cm^{-2}) and another with an

Figure 1. Temperature dependence of sheet resistance for selected 2DEGs formed at the a-LAO/KTO interfaces, measured with and without light illumination (light power has been set to 40 mW). The sudden drop in R_S around 50 K marks the effect of photo excitation. Labels in the figure mark the total carrier density deduced from the Hall effect. Inset in (d) is a sketch for experiment setup.

Figure 2. Hall resistance as a function of magnetic field, measured at 5 K by fixing light power to a series of constant values between 0 and 40 mW for the 2DEGs with (a) the lowest carrier density and (d) an intermediate carrier density. (b and c) The corresponding carrier density and Hall mobility, respectively, as functions of light power deduced from the data in (a). (e and f) The corresponding carrier density and Hall mobility for each species of charge carriers, deduced by fitting the experimental data in (d) to the two-band model. For clarity, we only show the result of curve fitting for the experimental data for P = 40 mW (cyan line) in (d).

intermediate n_S (4.5×10^{13} cm^{-2}). All R_{XY}-H curves were recorded at 5 K, obtained by keeping light power at a series of constant values between 0 and 40 mW. To avoid possible effects of illumination history, the sample was heated to room temperature and then to 5 K again before each measurement. Well linear R_{XY}−H relations are observed for the low carrier density sample (Figure 2a). This is the typical feature of the 2DEGs with only one species of charge carriers. The declining of the R_{XY}−H slope under light illumination indicates the appearance of extra charge carriers. A direct calculation gives the carrier density of $n_S = 0.2 \times 10^{13}$ cm^{-2} and $\sim 0.85 \times 10^{13}$ cm^{-2} before and after an illumination of $P = 40$ mW (Figure 2b). Photo excitation results in a density increase by 0.65×10^{13} cm^{-2}. Correspondingly, the Hall mobility grows from ~ 2104.4 cm^2/(V s) to ~ 3284.8 cm^2/(V s) (Figure 2c). These are the anticipated effects of photo excitation.

For the second specimen, in contrast, photo excitation modifies the Hall effect in a completely different manner. Instead of simply declining the R_{XY}−H slope, it causes a linear to nonlinear transition. As shown in Figure 2d, a sizable hump superimposing on a linear background appears in the low-field range of the R_{XY}−H curve and develops with the increase of light intensity. Finally, a stepwise R_{XY}−H relation results.

This illumination-caused unusual effect has never been observed before for the 2DEGs.[14−17] There are two possible explanations for this observation. The first one is the occurrence of anomalous Hall effect and the second one is the appearance of a second species of sheet charge carriers. After a careful analysis, we found that the two-band model gives a satisfactory description to the nonlinear Hall effect:[29]

$$R_{XY}(H) = -\frac{1}{e} \frac{\left(\frac{n_{s1}\mu_1^2}{1+\mu_1^2 H^2} + \frac{n_{s2}\mu_2^2}{1+\mu_2^2 H^2}\right)H}{\left(\frac{n_{s1}\mu_1}{1+\mu_1^2 H^2} + \frac{n_{s2}\mu_2}{1+\mu_2^2 H^2}\right)^2 + \left(\frac{n_{s1}\mu_1^2}{1+\mu_1^2 H^2} + \frac{n_{s2}\mu_2^2}{1+\mu_2^2 H^2}\right)^2 H^2}$$

(1)

with the constraint of

$$R_S(0) = \frac{1}{e(n_{S1}\mu_1 + n_{S2}\mu_2)}$$

(2)

where n_{S1} and n_{S2} demote, respectively, type one and type two sheet carriers at the a-LAO/KTO interface, μ_1 and μ_2 are the corresponding Hall mobilities, and e is electron charge. Obviously, $n_S = n_{S1}$ when there is only one species of sheet carriers and $n_S = n_{S1} + n_{S2}$ when two species of charge carriers coexist. As an example, in Figure 2d we show the result of curve fitting to the experimental data for $P = 40$ mW. The calculated results nicely reproduce the experimental ones adopting appropriate parameters (the $R_S(0)$ values required by data fitting are presented in Supporting Information Figure S4). Very good curve fittings are also obtained for other data and are not presented here for clarity.

A further analysis indicates that photo excitation has generated a second kind of charge carriers that have different characters from the original carriers. In Figure 2e,f we present the deduced carrier density and mobility for each species of charge carriers, respectively. Only one kind of charge carrier with a density around $n_{S1} \sim 4.5 \times 10^{13}$ cm^{-2} is observed in weak light (Figure 2e). When light power exceeds 10 mW, however, a second species of charge carrier appears, with its density growing from $n_{S2} \sim 3.0 \times 10^{10}$ to 1.8×10^{12} cm^{-2} as light intensity increases from 10 to 40 mW. Interestingly, the mobility of the extra charge carriers is much higher than that of

the original ones. According to Figure 2f, μ_2 is ~ 7600 cm^2/(V s), while μ_1 is only ~ 154 cm^2/(V s); the former is nearly 50-fold enhanced. Although two species of charge carriers were sometimes reported for the LAO/STO 2DEGs prepared under low oxygen pressures, the difference in their mobilities is generally around 1 order of magnitude.[29] The unusually large difference in mobility observed here reveals the distinct effect of photo excitation.

Figure 3a,b shows illumination-induced variations in respective carrier density and mobility for the samples with
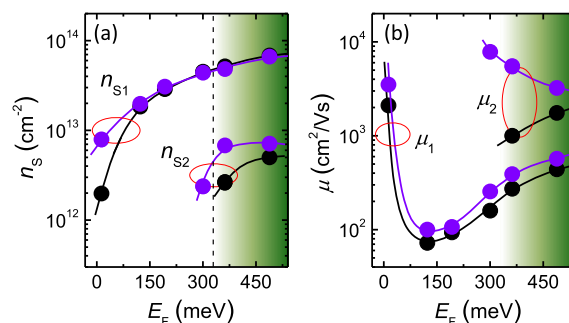
Figure 3. (a) Composition of the sheet charge carriers in different samples which are characterized by their Fermi energies, where the $n_S = n_{S1} + n_{S2}$ values in dark have been adopted for the calculation of E_F. From sample to sample, the Fermi energy varies in a wide range from ~ 13 meV to ~ 488 meV. The black and purple symbols represent the results without and with light illumination, respectively. Dashed line marks the band filling state around which photo excitation generates a second species of charge carriers with high mobility. (b) Corresponding mobilities. Solid lines are guides for the eye.

different Fermi energies. A threshold energy level can be clearly seen ($E_F \sim 333$ meV as marked by a dashed line in Figure 3a), which separates the 2DEGs composed of one and two species of mobile electrons. For the samples with the Fermi energy well above or well below this level, photo excitation does not change the species of mobile electrons, only tuning the already existed sheet charge carriers. Slightly below this energy level, however, light illumination produces an additional species of charge carriers with the highest mobility. Meanwhile, light illumination gains the strongest effect there. Presumably, above a threshold filling level electrons begin to occupy additional energy band thus behave differently.

According to Figure 3a, the photo-induced carrier density enhancement is much stronger when n_S is very low. In general, the charge carriers in 2DEGs mainly come from the in-gap states of KTO. Since the photon energy adopted in the present experiment (~ 3.1 eV) is smaller than the band gap of KTO (~ 3.5 eV), light illumination can only excite the occupied in-gap states in KTO. In general, the density of the occupied in-gap states will be lower for the sample with a high carrier density. This is why the photo-induced carrier density enhancement is stronger for low carrier density 2DEG than for high carrier density 2DEG.

The different mobilities of these two species of charge carriers deserve special attention. Without illumination, μ_1 and μ_2 are different by nearly a constant factor of ~ 3.7. Notably, light illumination speeds up μ_2 more rapidly than it does for μ_1, especially for the 2DEGs around the threshold energy level, making the two species of charge carriers more different.

Above a threshold energy level, as will be seen later, photocarriers spill over the d_{XY} band, starting to fill into d_{YZ}/d_{XZ} bands. Electrons in these latter two bands are more extended into the interior of KTO thus free from interfacial scattering.

To reveal the effect of band filling on SOC, the magnetoresistance of the 2DEGs is measured at 5 K in fields perpendicular to film plane. As an example, in Figure 4a−c, we
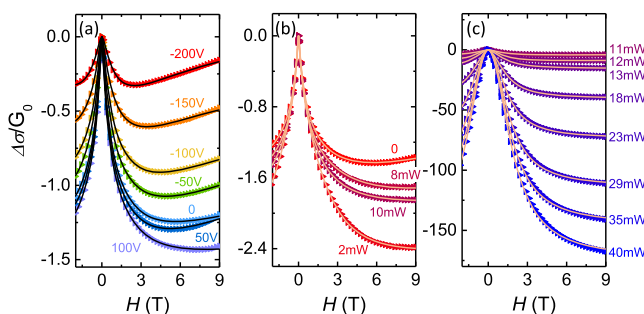
Figure 4. Magnetoconductance as a function of magnetic field applied in perpendicular to sample plane (symbols), measured at 5 K while electrically gating (a) or photo exciting the 2DGEs (b) and (c). Solid lines are results obtained by data fitting to eq 3, based on which the quantum correction associated with Rashba SOC to transport behavior can be determined.

present the magnetoconductance $\Delta\sigma(H) = \sigma(H) - \sigma(0)$ in unit of $G_0 = e^2/\pi h$ for the 2DEG with the specific density (4.5×10^{13} cm^{-2}) just below the threshold Fermi energy. Data for other 2DEGs can be found in Supporting Information Figure S5. To tune Fermi energy as strongly as possible, photo exciting and electrostatic gating were applied to the 2DEG in sequence, expanding the carrier density from 2.7×10^{13} cm^{-2} to 5.0×10^{13} cm^{-2}. With the increase of magnetic field, as shown in Figure 4a, the conductance exhibits first a rapid decrease and then a gradual increase when the 2DEG is negatively gated. This is the typical feature of antiweak localization and weak localization, originating from the quantum interference of the coherent electronic waves in the presence of spin relaxation associated with Rashba SOC. As carrier density increases from 2.7×10^{13} cm^{-2} to 4.5×10^{13} cm^{-2} (corresponding to a change in gate bias from −200 to 100 V), antiweak localization is enhanced, implying a variation in Rashba SOC. Further expanding carrier density up to 5.0×10^{13} cm^{-2} by photo excitation, antiweak localization (corresponding to $P = 18$ mW) remains sizable though the effect of weak localization has been completely counteracted by orbital magnetoresistance. When $P > 18$ mW, the $\Delta\sigma(H)$ cusp around $H = 0$ is no longer sharp since the orbital effect is dominative now. This is consistent with the results in Figures 1b and 2e,f, which show that the transport behavior is determined by highly mobile photocarriers in intensive light.

To get a quantitative description of SOC, we performed a further analysis of the $\Delta\sigma−H$ relation on the basis of the Maekawa−Fukuyama (MF) formula:[19,30]

$$\frac{\Delta\sigma(H)}{G_0} = -\Psi\left(\frac{1}{2} + \frac{H_{tr}}{H}\right) + \frac{3}{2}\Psi\left(\frac{1}{2} + \frac{H_i + H_{so}}{H}\right) - \frac{1}{2}\Psi\left(\frac{1}{2} + \frac{H_i}{H}\right)$$
$$- \left[\ln\left(\frac{H_i + H_{so}}{H_{tr}}\right) + \frac{1}{2}\ln\left(\frac{H_i + H_{so}}{H_i}\right)\right] - A_K \frac{\sigma(0)}{G_0}\frac{H^2}{1 + CH^2}$$

(3)

where $\Psi(x)$ is the digamma function defined as $\Psi(x) = \ln(x) + \Psi(1/2 + 1/x)$, and H_{tr}, H_i, and H_{SO} are the effective fields related to elastic scattering, inelastic scattering, and spin−orbit scattering, respectively. The quantum corrections to electronic conductance in the two-dimensional limit are described by the first four terms, and the last term is the Kohler term that simulates the orbital effect of magnetic field.

As shown by the solid curves in Figure 4, eq 3 well reproduces the experimental results (symbols) adopting appropriate fitting parameters. Satisfactory data fittings are also obtained for other samples with different Fermi energy (Supporting Information Figure S5). These results reveal the strong quantum corrections to magnetoresistance, thus allowing a full exploration for the effect of band filling on SOC. Figure 5a exemplifies the effective spin−orbit field (H_{SO})
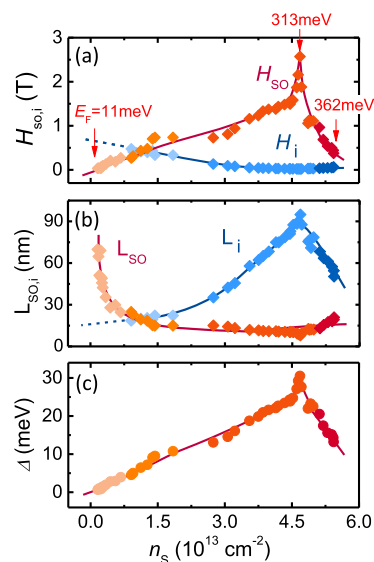
Figure 5. (a) Effective spin−orbit field and inelastic field, (b) spin precession distance and dephasing length, and (c) Rashba spin splitting energy as functions of carrier density. Results of different samples are represented by differently colored symbols. Solid lines are guides for the eye.

determined by data fitting, as a function of carrier density; here the results of different samples are represented by differently colored symbols. H_{SO} displays a strong dependence on the state of band filling. As n_S changes in the range from 0.16×10^{13} cm^{-2} to 4.5×10^{13} cm^{-2}, corresponding to the Fermi energy from 11 to 300 meV, H_{SO} grows monotonically from 0.03 to 1.6 T. Beyond this range, surprisingly, H_{SO} varies dramatically even for a very small increase of $\Delta n_S = 0.38 \times 10^{13}$ cm^{-2}, showing first a sharp jump from 1.6 to 2.6 T and a following abrupt drop to 1.1 T. Further increase in n_S leads to a rapid decay of H_{SO}. Notably, the sudden H_{SO} drop occurs accompanying the emergence of the highly mobile charge carriers. We doubly checked the cusp at the $H_{SO}−n_S$ curves and found it is a real feature of our 2DEGs (Supporting Information Figure S6). As will be seen later, this could be an indication for the charge carriers to spill over the d_{XY} band and fill into the d_{XZ}/d_{YZ} bands. H_{SO} is not shown for higher carrier densities ($P > 18$ mW) where orbital magnetoresistance is too large to reliably estimate H_{SO}. For the LAO/STO 2DEG, around the $d_{XY}−d_{XZ}/d_{YZ}$ crossing point of the band structure, H_{SO} exhibits a broad maximum due to enhanced spin

splitting.[17,33] The H_{SO} cusp for the a-LAO/KTO 2DEG deserves special attention. It suggests a difference in band structure from the LAO/STO interface, which has been confirmed by the later density functional theory calculations.

In Figure 5a we also show the effective field related to inelastic scattering (H_i). H_i is considerably smaller than H_{SO} when carrier density is high, implying the dominative role of antiweak localization in this regime. With the decrease of band filling, however, difference between H_i and H_{SO} continuously reduces, signifying the crossover from antiweak to weak localization.

Figure 5b shows the spin precession distance (L_{SO}) and dephasing length (L_i), as functions of carrier density, where $L_{i,SO}$ are determined by the fitting parameters $H_{i,SO}$ from the relation $L_{i,SO} = \sqrt{\hbar/4eH_{i,SO}}$. L_{SO} takes the values between 8 and 15 nm in a wide n_S range from 5.4×10^{13} cm^{-2} to 1.4×10^{13} cm^{-2}. However, as n_S decreases from 1.4×10^{13} cm^{-2} to 0.16×10^{13} cm^{-2}, L_{SO} displays a drastic increase from 15 to 70 nm, without signatures of saturation with further decreasing n_S. Therefore, the a-LAO/KTO 2DEG with a low band filling is a potential medium for spin transport. In this kind of 2DEG, spin precession distance is not only long but also extremly susceptible for n_S, which can be effectively tuned by electric gate or photo excitation.

In contrast to L_{SO}, the dephasing length displays an opposite dependence on carrier density, and its maximal value of 90 nm is reached at the n_S where L_{SO} is minimal. The Rashba spin splitting energy Δ can be further obtained from the relation $\Delta = 2\alpha k_F$, where the Rashba constant α is determined by $\tau_{SO} = \hbar^4/4\alpha^2 m_e^2 2D$, where $\tau_{SO} = L_{SO}^2/D$ is spin relaxation time, $D = v_F^2\tau_e/2$ the diffusion coefficient, $v_F = \hbar k_F/m_e$ the Fermi velocity, $k_F = \sqrt{2\pi n_s}$ the Fermi wave vector, $\tau_e = m_e\mu/e$ the elastic scattering time, and $m_e = 0.36m_0$, with m_0 being electron mass. Figure 5c shows the variation of the Rashba spin splitting energy with band filling. The maximal value is $\Delta = 30.5$ meV, larger than that of the LAO/STO 2DEG by a factor of 3.[10]

To get a deep understanding of the unusual tuning effect on 2DEGs, density functional theory calculations were performed adopting the method and model described in Experimental Section. Figure 6 shows the calculated orbital-resolved band structures of the KTO surface with the spin−orbit interaction taken into account. The size of green, blue, and red bubbles on the dispersion curve indicate the weight contribution of d_{XY} (green), d_{YZ} (blue), and d_{XZ} (red) orbitals. The lowest two bands near the Γ point are mainly from the d_{XY} orbitals of the first two TaO$_2$ monolayers from surface. The second band from inner TaO$_2$ layers is 0.22 eV from conduction band bottom. The lowest bands from d_{YZ} and d_{XZ}, ∼0.47 eV above the conduction band bottom, are extended along the z axis, in contrast to the d_{XY} bands localized mainly in the TaO$_2$ monolayers. Rashba splitting is invisible in the d_{XY} bands but very strong for the d_{XZ}/d_{YZ} bands, resulting in a left and a right band shift in Figure 6b,c. A further analysis gives the wave vector offset of $k_0 = 0.07$ A^{-1} and the Rashba energy of $E_R = 10.8$ meV (Figure 6b).[31,32] A striking feature deserving special attention is the deviation of the dispersion curve from the parabolic form for the d_{YZ}/d_{XZ} states. This leads to a rapid decrease of spin splitting as E_F increases (Supporting Information Figure S7), that is, considerably SOC exists only in the green region marked in Figure 6b. This is different from the LAO/STO 2DEG, for which the dispersion relation is always parabolic.[33]
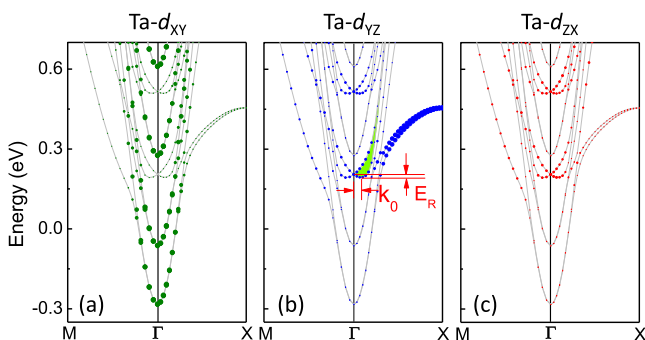
On the basis of the calculated band structure, we can understand the experimental results. Mobile electrons will first occupy the low-level d_{XY} states near KTO surface. In this case, the Rashba SOC is weak, which explains the long spin precession distance when n_S is low. As Fermi energy closes to a threshold value, however, a portion of the electrons starts to fill into the d_{XZ}/d_{YZ} orbitals, resulting in a sudden growth in Rashba SOC thus in H_{SO}. The subsequent decrease in H_{SO} could be ascribed to the reduced spin splitting of the d_{ZX}/d_{YZ} bands as Fermi energy grows. From the results of band calculation, we can evaluate the Rashba constant $\alpha = 2E_R/k_0$. For the KTO structure, the deduced α is 0.31 eVÅ, in reasonable agreement with the experimental value ∼0.1 eVÅ.

The calculated threshold n_S for the largest Rashba SOC is 2.0×10^{14} cm^{-2}, while the observed n_S is ∼4.7×10^{13} cm^{-2}. This discrepancy could be due to the oversimplified model for theoretical calculation. An uniform TaO$_2$ terminal layer has been adopted by this model, while the practical one could be a mixture of TaO$_2$ and KO.

Finally, we would like to present a brief comparison between the 2DEGs composed of 5d and 3d electrons. Compared with 3d 2DEGs, 5d 2DEGs have two distinct features. First, their Hall mobility is generally high since 5d electrons have a wider bandwidth than the 3d ones. Second, the spin−orbit energy splitting is obviously large due to the strong atomic SOC of KTO. Allof these features will allow the exploration of high performance 2DEGs with quantum effect and tunable spin relaxation that is highly desired by spintronics.

Figure 6. Electronic bands of KTO surface with spin−orbit interaction and their predominant orbital characters marked by differently colored bubbles. The size of the bubbles represents the weight contribution. Shaded area in (b) marks effect of spin splitting. Band dispersions are shown along the interface (XY plane) with $X = \pi/a(1,0,0)$ and $M = \pi/a(1,1,0)$, where a is the in-plane lattice constant.

CONCLUSION

In summary, effects of electric and optical tuning to KTO-based 2DEGs with totally different band fillings have been investigated. A relationship between the effective Rashba SOC field and band filling has been established in the Fermi energy range from ∼13 meV to ∼362 meV, showing that the maximal spin precession length is 70.1 nm and the maximal Rashba spin splitting energy is 30 meV. The most important observation is the presence of a critical band filling where the Rashba SOC gets a sharp peak and the composition of mobile electrons undergoes a crossover from one to two species as Fermi energy exceeds this filling level. As evidenced by density functional theory calculation, these unusual observations are closely associated with the distinct hierarchic band structure of

$KTaO_3$-based 2DGEs. The present work reveals the special characters of 5d 2DEGs, deepening our understanding of the low-dimensional electron system.

EXPERIMENTAL SECTION

Sample Fabrication. The 2DEG was fabricated by growing an amorphous $LaAlO_3$ (a-LAO) layer of 10 nm on (001)-oriented KTO single crystal substrate by pulsed laser deposition (λ = 248 nm) with a single crystalline LAO target. The repetition rate is 2 Hz, and the laser fluence is 2 J/cm^2. In the deposition process, by varying the substrate temperature (T_S) and the oxygen pressure (P_{O_2}) during growth (details in Supporting Information), we obtained the 2DEGs with different band filling. After deposition, the film was naturally cooled down to room temperature without changing the oxygen atmosphere. Film thickness was determined by the number of laser pulses, with the deposition rate has been calibrated by small-angle X-ray reflectivity.

Structural and Resistive Measurements. Surface morphology of the heterostructure was measured by atomic force microscope (AFM, SPI 3800N, Seiko). Crystal structure of the films was determined by a Bruker X-ray diffractometer equipped with thin-film accessories (D8 Discover, Cu Kα radiation). Lattice images were recorded by a high-resolution scanning transmission electron microscope with double C_S correctors (JEOL-ARM200F). Both longitudinal and transverse resistances were measured, using a quantum-designed physical property measurement system (PPMS) in the magnetic field perpendicular to the sample plane. An applied current of 10 μA was for the measurement. Ultrasonic wire bonding (Al wires of 20 μm in diameter) was used for electric contacts. The Hall-bar-shaped sample (200 × 1200 μm^2) was adopted for the electric measurement. To investigate gating effect, an electric voltage was applied to a copper back gate, while the a-LAO/KTO interface was grounded. The leakage current was lower than 10 nA. To investigate the effect of photo excitation, a laser beam (λ = 405 nm) was introduced into PPMS by an optical fiber. The spot size of the light was ~2 mm in diameter.

Density Functional Theory Calculations. First-principles calculations were performed using the projector-augmented wave method within the density functional theory,[34,35] as implemented in the Vienna ab Initio Simulation Package (VASP).[36,37] We use the generalized gradient approximation functional (PBEsol) improved for solids and their surfaces.[38,39] Because KTO has much larger electron affinity than LAO and the LAO layer is amorphous, we use a slab model of $(KTO)_m$ with m = 11 unit cells to describe the effective electron carriers in the LAO/KTO system. The KTO slab structure is fully optimized with in-plane lattice constant constrained to the experimental lattice constants using a Γ-centered 4 × 4 × 1 k-grid. The plane wave energy cutoff is set to 500 eV. A 20 Å-thick vacuum layer ensures decoupling in the slab geometry. The in-plane lattice constant is the experimental lattice constant of KTO with 3.989 Å, and the out-of-plane lattice constant and all the internal atomic positions are allowed to relax sufficiently. Our convergence standard requires that the Hellmann–Feynmann force on each atom is <0.01 eV/Å and the absolute total energy difference between two successive loops is smaller than 10^{-5} eV. The electronic structure calculations were performed by using a Γ-centered 8 × 8 × 1 k-grid with the spin–orbit coupling included.

ASSOCIATED CONTENT

Ⓢ Supporting Information

The Supporting Information is available free of charge on the ACS Publications website at DOI: 10.1021/acsnano.8b07622.

> Details of the procedures for 2DEGs fabricated at the a-LAO/KTO interfaces, the rectify-shaped anisotropic magnetoresistance, magnetoresistance and zero-field resistance $R_S(0)$ for the 2DEG with a n_S of 4.5 × 10^{13} cm^{-2}, the results of data fitting of magnetoconductance for other samples with different fillings and spin splitting

between the two Rashba bands as a function of energy (PDF)

AUTHOR INFORMATION

Corresponding Author
*E-mail: jrsun@iphy.ac.cn.

ORCID Ⓞ
Jine Zhang: 0000-0001-7949-3239
Banggui Liu: 0000-0002-6030-6680
Jirong Sun: 0000-0003-1238-8770

Notes
The authors declare no competing financial interest.

REFERENCES

(1) Ohtomo, A.; Hwang, H. Y. A High-Mobility Electron Gas at the LaAlO$_3$/SrTiO$_3$ Heterointerface. *Nature* **2004**, *427*, 423−426.

(2) Nakagawa, N.; Hwang, H. Y.; Muller, D. A. Why Some Interfaces Cannot Be Sharp. *Nat. Mater.* **2006**, *5*, 204−209.

(3) Herranz, G.; Basletic, M.; Bibes, M.; Carretero, C.; Tafra, E.; Jacquet, E.; Bouzehouane, K.; Deranlot, C.; Hamzic, A.; Broto, J. M.; Barthelemy, A.; Fert, A. High Mobility in LaAlO$_3$/SrTiO$_3$ Heterostructures: Origin, Dimensionality, and Perspectives. *Phys. Rev. Lett.* **2007**, *98*, 216803.

(4) Kalabukhov, A.; Gunnarsson, R.; Borjesson, J.; Olsson, E.; Claeson, T.; Winkler, D. Effect of Oxygen Vacancies in the SrTiO$_3$ Substrate on the Electrical Properties of the LaAlO$_3$/SrTiO$_3$ Interface. *Phys. Rev. B: Condens. Matter Mater. Phys.* **2007**, *75*, 121404.

(5) Reyren, N.; Thiel, S.; Caviglia, A. D.; Kourkoutis, L. F.; Hammerl, G.; Richter, C.; Schneider, C. W.; Kopp, T.; Ruetschi, A. S.; Jaccard, D.; Gabay, M.; Muller, D. A.; Triscone, J. M.; Mannhart, J. Superconducting Interfaces Between Insulating Oxides. *Science* **2007**, *317*, 1196−1199.

(6) Brinkman, A.; Huijben, M.; Van Zalk, M.; Huijben, J.; Zeitler, U.; Maan, J. C.; Van der Wiel, W. G.; Rijnders, G.; Blank, D. H. A.; Hilgenkamp, H. Magnetic Effects at the Interface Between Non-Magnetic Oxides. *Nat. Mater.* **2007**, *6*, 493−496.

(7) Thiel, S.; Hammerl, G.; Schmehl, A.; Schneider, C. W.; Mannhart, J. Tunable Quasi-Two-Dimensional Electron Gases in Oxide Heterostructures. *Science* **2006**, *313*, 1942−1945.

(8) Bell, C.; Harashima, S.; Kozuka, Y.; Kim, M.; Kim, B. G.; Hikita, Y.; Hwang, H. Y. Dominant Mobility Modulation by the Electric Field Effect at the LaAlO$_3$/SrTiO$_3$ Interface. *Phys. Rev. Lett.* **2009**, *103*, 226802.

(9) Caviglia, A. D.; Gariglio, S.; Cancellieri, C.; Sacepe, B.; Fete, A.; Reyren, N.; Gabay, M.; Morpurgo, A. F.; Triscone, J. M. Two-Dimensional Quantum Oscillations of the Conductance at LaAlO$_3$/SrTiO$_3$ Interfaces. *Phys. Rev. Lett.* **2010**, *105*, 236802.

(10) Caviglia, A. D.; Gabay, M.; Gariglio, S.; Reyren, N.; Cancellieri, C.; Triscone, J. M. Tunable Rashba Spin-Orbit Interaction at Oxide Interfaces. *Phys. Rev. Lett.* **2010**, *104*, 126803.

(11) Ariando, A.; Wang, X.; Baskaran, G.; Liu, Z.; Huijben, J.; Yi, J.; Annadi, A.; Barman, A. R.; Rusydi, A.; Dhar, S.; Feng, Y.; et al. Electronic Phase Separation at the LaAlO$_3$/SrTiO$_3$ Interface. *Nat. Commun.* **2011**, *2*, 188.

(12) Lesne, E.; Fu, Y.; Oyarzun, S.; Rojas-Sanchez, J. C.; Vaz, D. C.; Naganuma, H.; Sicoli, G.; Attane, J. P.; Jamet, M.; Jacquet, E.; George, J. M.; Barthelemy, A.; Jaffres, H.; Fert, A.; Bibes, M.; Vila, L. Highly

Efficient and Tunable Spin-to-Charge Conversion Through Rashba Coupling at Oxide Interfaces. *Nat. Mater.* **2016**, *15*, 1261−1266.

(13) Song, Q.; Zhang, H.; Su, T.; Yuan, W.; Chen, Y.; Xing, W.; Shi, J.; Sun, J.; Han, W. Observation of Inverse Edelstein Effect in Rashba-Split 2DEG Between SrTiO₃ and LaAlO₃ at Room Temperature. *Sci. Adv.* **2017**, *3*, e1602312.

(14) Tebano, A.; Fabbri, E.; Pergolesi, D.; Balestrino, G.; Traversa, E. Room-Temperature Giant Persistent Photoconductivity in SrTiO₃/LaAlO₃ Heterostructures. *ACS Nano* **2012**, *6*, 1278−1283.

(15) Lei, Y.; Li, Y.; Chen, Y. Z.; Xie, Y. W.; Chen, Y. S.; Wang, S. H.; Wang, J.; Shen, B. G.; Pryds, N.; Hwang, H. Y.; Sun, J. R. Visible-Light-Enhanced Gating Effect at the LaAlO₃/SrTiO₃ Interface. *Nat. Commun.* **2014**, *5*, 5554.

(16) Liu, G. Z.; Qiu, J.; Jiang, Y. C.; Zhao, R.; Yao, J. L.; Zhao, M.; Feng, Y.; Gao, J. Light Induced Suppression of Kondo Effect at Amorphous LaAlO₃/SrTiO₃ Interface. *Appl. Phys. Lett.* **2016**, *109*, 031110.

(17) Cheng, L.; Wei, L.; Liang, H.; Yan, Y.; Cheng, G.; Lv, M.; Lin, T.; Kang, T.; Yu, G.; Chu, J.; Zhang, Z.; Zeng, C. Optical Manipulation of Rashba Spin-Orbit Coupling at SrTiO₃-Based Oxide Interfaces. *Nano Lett.* **2017**, *17*, 6534−6539.

(18) Ben Shalom, M.; Sachs, M.; Rakhmilevitch, D.; Palevski, A.; Dagan, Y. Tuning Spin-Orbit Coupling and Superconductivity at the SrTiO₃/LaAlO₃ Interface: A Magnetotransport Study. *Phys. Rev. Lett.* **2010**, *104*, 126802.

(19) Herranz, G.; Singh, G.; Bergeal, N.; Jouan, A.; Lesueur, J.; Gazquez, J.; Varela, M.; Scigaj, M.; Dix, N.; Sanchez, F.; Fontcuberta, J. Engineering Two-Dimensional Superconductivity and Rashba Spin-Orbit Coupling in LaAlO₃/SrTiO₃ Quantum Wells by Selective Orbital Occupancy. *Nat. Commun.* **2015**, *6*, 6028.

(20) Niu, W.; Zhang, Y.; Gan, Y. L.; Christensen, D. V.; Soosten, M. V.; Garcia-Suarez, E. J.; Riisager, A.; Wang, X. F.; Xu, Y. B.; Zhang, R.; Pryds, N.; Chen, Y. Z. Giant Tunability of the Two-Dimensional Electron Gas at the Interface of Gamma-Al₂O₃/SrTiO₃. *Nano Lett.* **2017**, *17*, 6878−6885.

(21) Uwe, H.; Oka, K.; Unoki, H.; Sakudo, T. Raman Scattering From Conduction Electron in KTaO₃. *J. Phys. Soc. Jpn.* **1980**, *49*, 577−580.

(22) Uwe, H.; Sakudo, T.; Yamaguchi, H. Interband Electronic Raman Scattering in SrTiO₃. *Jpn. J. Appl. Phys.* **1985**, *24*, 519.

(23) Nakamura, H.; Kimura, T. Electric Field Tuning of Spin-Orbit Coupling in KTaO₃ Field-Effect Transistors. *Phys. Rev. B: Condens. Matter Mater. Phys.* **2009**, *80*, 121308.

(24) Harashima, S.; Bell, C.; Kim, M.; Yajima, T.; Hikita, Y.; Hwang, H. Y. Coexistence of Two-Dimensional and Three-Dimensional Shubnikov-de Haas Oscillations in Ar+-Irradiated KTaO₃. *Phys. Rev. B: Condens. Matter Mater. Phys.* **2013**, *88*, 075434.

(25) Santander-Syro, A. F.; Bareille, C.; Fortuna, F.; Copie, O.; Gabay, M.; Bertran, F.; Taleb-Ibrahimi, A.; Le Fevre, P.; Herranz, G.; Reyren, N.; Bibes, M.; Barthelemy, A.; Lecoeur, P.; Guevara, J.; Rozenberg, M. J. Orbital Symmetry Reconstruction and Strong Mass Renormalization in the Two-Dimensional Electron Gas at the Surface of KTaO₃. *Phys. Rev. B: Condens. Matter Mater. Phys.* **2012**, *86*, 121107.

(26) King, P. D. C.; He, R. H.; Eknapakul, T.; Buaphet, P.; Mo, S. K.; Kaneko, Y.; Harashima, S.; Hikita, Y.; Bahramy, M. S.; Bell, C.; Hussain, Z.; Tokura, Y.; Shen, Z. X.; Hwang, H. Y.; Baumberger, F.; Meevasana, W. Subband Structure of a Two-Dimensional Electron Gas Formed at the Polar Surface of the Strong Spin-Orbit Perovskite KTaO₃. *Phys. Rev. Lett.* **2012**, *108*, 117602.

(27) Zou, K.; Ismail-Beigi, S.; Kisslinger, K.; Shen, X.; Su, D.; Walker, F. J.; Ahn, C. H. LaTiO₃/KTaO₃ Interfaces: A New Two-Dimensional Electron Gas System. *APL Mater.* **2015**, *3*, 036104.

(28) Zhang, H.; Zhang, H.; Yan, X.; Zhang, X.; Zhang, Q.; Zhang, J.; Han, F.; Gu, L.; Liu, B.; Chen, Y.; Shen, B.; Sun, J. Highly Mobile Two-Dimensional Electron Gases with a Strong Gating Effect at the Amorphous LaAlO₃/KTaO₃ Interface. *ACS Appl. Mater. Interfaces* **2017**, *9*, 36456−36461.

(29) Gunkel, F.; Bell, C.; Inoue, H.; Kim, B.; Swartz, A. G.; Merz, T. A.; Hikita, Y.; Harashima, S.; Sato, H. K.; Minohara, M.; Hoffmann-Eifert, S.; Dittmann, R.; Hwang, H. Y. Defect Control of Conventional and Anomalous Electron Transport at Complex Oxide Interfaces. *Phys. Rev. X* **2016**, *6*, 031035.

(30) Maekawa, S.; Fukuyama, H. Magnetoresistance in Two-Dimensional Disordered-Systems-Effects of Zeeman Splitting and Spin-Orbit Scattering. *J. Phys. Soc. Jpn.* **1981**, *50*, 2516−2524.

(31) Ast, C. R.; Henk, J.; Ernst, A.; Moreschini, L.; Falub, M. C.; Pacile, D.; Bruno, P.; Kern, K.; Grioni, M. Giant Spin Splitting Through Surface Alloying. *Phys. Rev. Lett.* **2007**, *98*, 186807.

(32) Wang, T. H.; Jeng, H. T. Wide-Range Ideal 2D Rashba Electron Gas with Large Spin Splitting in Bi₂Se₃/MoTe₂ Heterostructure. *NPJ. Comput. Mater.* **2017**, *3*, 5.

(33) Zhong, Z.; Toth, A.; Held, K. Theory of Spin-Orbit Coupling at LaAlO₃/SrTiO₃ Interfaces and SrTiO₃ Surfaces. *Phys. Rev. B: Condens. Matter Mater. Phys.* **2013**, *87*, 161102.

(34) Hohenberg, P.; Kohn, W. Inhomogeneous Electron Gas. *Phys. Rev.* **1964**, *136*, B864.

(35) Kohn, W.; Sham, L. J. Self-Consistent Equations Including Exchange and Correlation Effects. *Phys. Rev.* **1965**, *140*, A1133.

(36) Kresse, G.; Joubert, D. From Ultrasoft Pseudopotentials to the Projector Augmented-Wave Method. *Phys. Rev. B: Condens. Matter Mater. Phys.* **1999**, *59*, 1758−1775.

(37) Blochl, P. E. Projector Augmented-Wave Method. *Phys. Rev. B: Condens. Matter Mater. Phys.* **1994**, *50*, 17953−17979.

(38) Perdew, J. P.; Burke, K.; Ernzerhof, M. Generalized Gradient Approximation Made Simple. *Phys. Rev. Lett.* **1996**, *77*, 3865−3868.

(39) Perdew, J. P.; Ruzsinszky, A.; Csonka, G. I.; Vydrov, O. A.; Scuseria, G. E.; Constantin, L. A.; Zhou, X.; Burke, K. Restoring the Density-Gradient Expansion for Exchange in Solids and Surfaces. *Phys. Rev. Lett.* **2008**, *100*, 136406.